JCTC Journal of Chemical Theory and Computation

pubs.acs.org/JCTC Article

Cost-Effective Approach for Modeling of Multiresonant Thermally Activated Delayed Fluorescence Emitters

Sanyam, Rudranarayan Khatua, and Anirban Mondal*

Cite This: https://doi.org/10.1021/acs.jctc.3c01147 Read Online

ACCESS | Metrics & More | Article Recommendations | Supporting Information

ABSTRACT: Multiresonant thermally activated delayed fluorescence (MR-TADF) emitters have recently attracted great interest for application in organic light-emitting diodes due to their remarkable electroluminescent efficiency and narrow emission spectra. It is therefore essential to establish computational methodologies that can accurately model the excited states of these materials at manageable computational costs. With regard to MR-TADF design and their associated photophysics, previous works have highlighted the importance of wave function-based methods, at much higher computational costs, over the traditional time-dependent density functional theory approach. Herein, we employ two independent techniques built on different quantum mechanical frameworks, highly correlated wave function-based STEOM-DLPNO−CCSD and range-separated double hybrid density functional, TD-B2PLYP, to investigate their performance in predicting the excited state energies in MR-TADF emitters. We demonstrate a remarkable mean absolute deviation (MAD) of ∼0.06 eV in predicting ΔE_{ST} compared to experimental measurements across a large pool of chemically diverse MR-TADF molecules. Furthermore, both methods yield superior MAD in estimating S_1 and T_1 energies over earlier reported SCS-CC2 computed values [*J. Chem. Theory Comput.* **2022,** 18, 4903]. The short-range charge-transfer nature of low-lying excited states and narrow fwhm values, hallmarks of this class of emitters, are precisely captured by both approaches. Finally, we show the transferability and robustness of these methods in estimating rates of radiative and nonradiative events with adequate agreement against experimental measurements. Implementing these cost-effective computational approaches is poised to streamline the identification and evaluation of potential MR-TADF emitters, significantly reducing the reliance on costly laboratory synthesis and characterization processes.

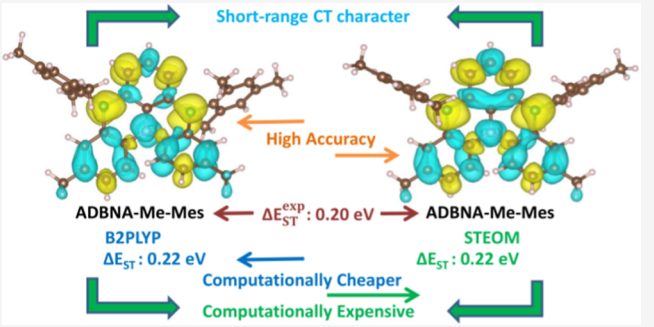

1. INTRODUCTION

Thermally activated delayed fluorescence (TADF) compounds have emerged as promising materials for next-generation organic light-emitting diodes (OLEDs) due to their efficient utilization of singlet and triplet excitons.[1−3] Although traditional donor−acceptor TADF systems have shown significant progress, the recent exploration of multiresonance TADF (MR-TADF) compounds has opened up new avenues for enhanced device performance. In the case of donor−acceptor−donor (D−A−D) type of TADF compounds, the highest occupied molecular orbital (HOMO) and lowest unoccupied molecular orbital (LUMO) are well separated due to highly twisted structure such that there is minimum exchange integral,[2,4−8] which yields minimum energy gap (ΔE_{ST}) between singlet and triplet states. Therefore, ΔE_{ST} in the case of D-A−D type molecules is very small. However, these emitters suffer from poor external quantum efficiency (EQE) due to considerable reorganization energies and low oscillator strength values.[9] In contrast, multiresonance TADF compounds are characterized by nanographene-like architecture with site-specific doping of electron-withdrawing moieties (e.g., boron and ketone groups) and electron-donating atoms (e.g., nitrogen and oxygen).[10] The opposite resonance effect induced by the electron-donating and -withdrawing groups reduces the exchange interaction and consequently ΔE_{ST}. These fused-ring MR compounds offer distinct advantages over traditional donor−acceptor TADF systems, e.g., large oscillator strength due to relatively larger overlap of the HOMO and LUMO; they possess color purity due to their rigid structure, i.e., emit in a narrow band range, have small Stokes's shift, and show minimal positive solvatochromism owing to the short-range charge transfer (SRCT) and perform better in terms of efficiency (EQE).[4,5,11−23]

Among the critical factors influencing the performance of TADF compounds, ΔE_{ST}, spin−orbit coupling ($H_{SO}^{S_1T_1}$), and reorganization energies (λ) play pivotal roles.[24] Over the past

Received: October 17, 2023
Revised: November 28, 2023
Accepted: November 28, 2023

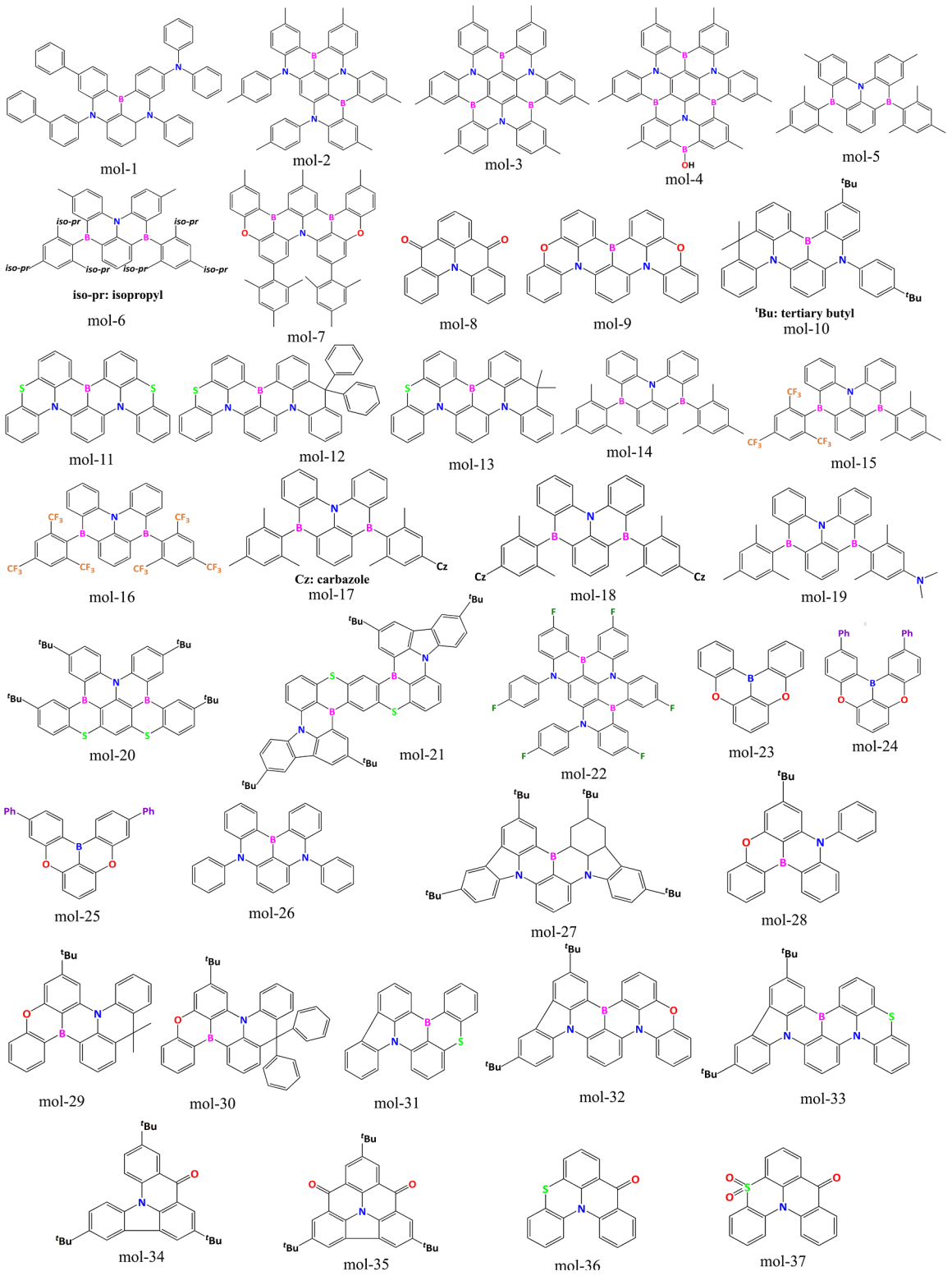

Figure 1. Chemical structures of all the experimentally known compounds investigated in this work.[12,15,16,23,47−58]

years, density functional theory (DFT) and its time-dependent (TD) variant have been widely used as the quantum mechanical method that provides an efficient and accurate approach to estimate ΔE_{ST} in traditional TADF compounds.[25] Within the TADF community, a range of exchange−correlation functionals have been used—starting from hybrid functionals such as B3LYP, PBE0, or M06-2X to range-separated functional that include CAM-B3LYP and LC-ωPBE.[26−30] Several reports have summarized the advantages of some DFT methods over others in predicting ΔE_{ST} in D−A−D systems.[25,31] However, when modeling MR-TADF emitters, the standard DFT functionals fail to predict both energies and associated rates dramatically.[32] Sancho-García and co-workers demonstrated the poor performance of

https://doi.org/10.1021/acs.jctc.3c01147
J. Chem. Theory Comput. XXXX, XXX, XXX−XXX

inherent single-excitation methods, including TD-DFT with generalized gradient approximation (GGA), *meta*-GGA, and hybrid functionals that predict a much larger ΔE_{ST}, which they have coined due to a poorer account of the Coulomb correlation.[32,33] In addition to electron correlation, it is understood that a proper account of double excitations plays a significant role in MR-TADFs. The primary reason behind the poor performance of these DFT functionals is that they lack double excitation information. Further, it was shown that the poor TD-DFT prediction of ΔE_{ST} can be overcome by deploying wave function-based methods such as the spin-component scaling second-order approximate coupled cluster (SCS-CC2) approach or coupled cluster calculations including higher-order excitations.[32] In a recent report, Hall et al. conducted a comprehensive quantum mechanical study on a large pool of MR-TADF molecules at the SCS-CC2/cc-pVDZ level of theory.[32] They obtained a remarkable mean average deviation (MAD) of 0.04 eV against the experimental data when computing ΔE_{ST}. Similar performance was seen by other wave function-based methods, such as scaled opposite-spin coupled cluster (SOS-CC2) and coupled cluster (CC2). On the other hand, in a related study, Shizu and Kaji highlighted the significance of the equation-of-motion coupled-cluster singles and doubles (EOM-CCSD) method.[34] They specifically investigated the DABNA-1[35] compound and observed a remarkable agreement between the predicted and experimental measurements not only for ΔE_{ST} but also quantitatively reproduced all rate constants relevant to the emission mechanism. In addition, methods like second-order algebraic diagrammatic construction ADC(2) and SCS-ADC(2) that include partially double excitation have also been successfully applied to MR-TADF.[36] Within the wave function-based framework, the (partial) inclusion of double excitations, which are omitted in TD-DFT, is responsible for the greater accuracy in predicting ΔE_{ST}, primarily attributed to a better description of the Coulomb correlation interaction. However, the improved accuracy owing to the inclusion of higher-order electronic excitations also leads to an increased computational overhead that could be a bottleneck when performing large-scale screening. Another practical challenge in working with the above-mentioned wave function-based methods is that most are unavailable to the open-source research community.

As reported recently by Brédas et al., the computational complexities described above can be addressed using the STEOM-DLPNO−CCSD method.[37,38] Similarity transformed equation of motion method augmented with domain-based on local pair natural orbitals (STEOM-DLPNO−CCSD) is a highly correlated wave function-based approach that can adequately account for the higher-order excitations (singles and doubles) and, hence, offers an accurate treatment for the excited state characteristics of various molecules, including (MR) TADF-based compounds while keeping manageable computational costs.[37,39,40] Although this computational approach has been successfully utilized recently to investigate ΔE_{ST}, $H_{SO}^{S_1T_1}$, and subsequently the rates of photophysical events in the MR-TADF compounds, no comprehensive benchmark studies are highlighting the accuracy compared to experimental measurements performed on a significant set of MR-TADF emitters. In addition, another efficient approach that includes double excitations is the double-hybrid TD-DFT,[41] which has been recently shown to perform adequately in predicting ΔE_{ST} of organic molecules with inverted gaps between first excited singlet and triplet states by Aspuru-Guzik and co-workers.[42] Although the range-separated double-hybrid TD-DFT approximation, such as ωB2PLYP, accounts for the double excitations for the excited singlet state, it is devoid of the perturbative doubles correction for the excited triplet energies.[43] However, it includes static and dynamic electron correlation and dispersion correction, providing a more accurate description of the electronic properties.

In this work, we aim to examine the performance of two independent approaches constructed on different frameworks, STEOM-DLPNO−CCSD and range-separated double-hybrid TD-DFT, in terms of their accuracy and applicability across a large and diverse pool of MR-TADF emitters. Toward this end, we have computed ΔE_{ST}, spin−orbit coupling, reorganization energies, radiative/nonradiative rates, and the nature of excited states of 37 reported MR-TADF complexes at STEOM-DLPNO−CCSD/def2-SVP and B2PLYP/def2-TZVP levels of theory. For completeness, we have also performed TD-DFT calculations employing a hybrid functional, TPSSh/6-31+G-(d,p). We used the MAD, root-mean-square deviation (RMSD), and standard deviation as the metric to quantify the accuracy of the prediction. Our study reveals that TD-DFT calculations with the hybrid functional (TPSSh) fail to predict accurate ΔE_{ST}. A satisfactory agreement with experimental ΔE_{ST} was observed by employing double excitation methods. Computed results exhibit a remarkable MAD of ∼0.06 eV for the predicted ΔE_{ST} across the investigated MR-TADF emitters when STEOM-DLPNO−CCSD or TD-B2PLYP techniques are used. The estimated rate constants for radiative and nonradiative events show adequate agreement with the available experimental measurements. Finally, we have also probed the nature of excited states based on the density difference plots. These plots revealed SRCT character for the examined MR-TADF complexes via both STEOM-DLPNO−CCSD and TD-B2PLYP approaches. Our results affirm the robustness of the two independent approaches for the predictions of excited state energies, rate constants, and the SRCT character of excited states, thus providing a cost-effective route for future investigations of MR-TADF emitters.

2. METHODS

2.1. Quantum Mechanical Calculations. We deployed a comprehensive computational approach to investigate 37 experimentally reported MR-TADF compounds in the literature. The chemical structures of these molecules are displayed in Figure 1. As used in the experimental reports, the corresponding names are mapped in Table S1 of the Supporting Information. The ground state (S_0) optimizations and frequency analysis for these complexes were carried out at the TPSSh/6-31+G(d,p) level of theory using the Gaussian09 program.[44] To account for solvent effects, dichloromethane (ϵ = 8.93) was considered using the conductor-like polarizable continuum (CPCM) solvent model.[45] The selection of the functional and PCM conditions was primarily driven by the recent reports from Gao et al.,[46] where the authors demonstrated that the TPSSh/6-31+G(d)-PCM model successfully reproduced the experimental DABNA-1 emission and absorption wavelengths in CH_2Cl_2.

For the accurate assessment of the energies of the singlet and triplet excited state manifolds, the corresponding energy gaps, and the spin−orbit couplings, we performed highly correlated wave function calculations at the STEOM-DLPNO−CCSD/def2-SVP level of theory. We considered

https://doi.org/10.1021/acs.jctc.3c01147
J. Chem. Theory Comput. XXXX, XXX, XXX−XXX

single and double excitations among five singlet or triplet excited states. The ground-state DFT-optimized geometries were utilized to perform single-point calculations to determine the energies of the singlet and triplet states and the related ΔE_{ST} values. Such protocol was employed primarily to control the computational overhead and was already shown to reproduce the experimental data reported for MR-TADF molecules accurately.[37,38] The def2-SVP basis set was used to a great extent to reduce the overall computational cost. We tested the convergence of the cutoff values used for the STEOM-DLPNO−CCSD calculation. The converged cutoff values used were `othresh` = 0.005, `vthresh` = 0.005, and `TCutPNOSingles` = 1×10^{-11}. In addition to these wave function-based calculations, excited state energies, the associated singlet−triplet energy gaps, and the spin−orbit couplings were computed using a double-hybrid functional, B2PLYP and def2-TZVP basis set. These wave function-based and B2PLYP double-hybrid calculations were performed with the ORCA v5.0.3 package.[59] Finally, for the sake of completeness, vertical ΔE_{ST} values were obtained using TPSSh/6-31+G(d,p) method. The solvent and solvent model used were consistent with the previous calculations.

We used the MAD, RMSD, and standard deviation (σ) as the metric to estimate the accuracy of the computed quantities across various methods. The following equations were used to determine these quantities.

$$\mathrm{MAD} = \frac{1}{n}\sum_{i=1}^{n} |x_i| \tag{1}$$

$$\mathrm{RMSD} = \sqrt{\frac{1}{n}\sum_{i=1}^{n} |x_i|^2} \tag{2}$$

$$\sigma = \sqrt{\left(\frac{1}{n}\sum_{i=1}^{n} |x_i|^2\right) - \left(\frac{1}{n}\sum_{i=1}^{n} |x_i|\right)^2} \tag{3}$$

where $x_i = y_i^{\text{experiment}} - y_i^{\text{theoretical}}$ with $y_i^{\text{experiment}}$ being either S_1, T_1, or ΔE_{ST} values obtained from experimental measurements refers to corresponding TPSSh, B2PLYP, and STEOM-DLPNO−CCSD computed values for S_1, T_1 or, ΔE_{ST} and i is the index over the series of 37 studied molecules.

The photophysical properties of the MR-TADF systems are examined via parameters such as rates of prompt-fluorescence (k_{PF}), intersystem crossing (k_{ISC}), and reverse intersystem crossing (k_{RISC}). The rate of prompt fluorescence, which occurs due to the radiative decay from the first singlet excited state, can be expressed using Einstein's formula[60] as follows.

$$k_{PF} = \frac{\Delta E_{S_0S_1}^2 f_{S_0S_1}}{1.499} \tag{4}$$

Here, $f_{S_0S_1}$ is the oscillator strength and $\Delta E_{S_0S_1}$ is the energy difference between S_0 and S_1 states in cm^{-1}. The rate constants of ISC (from S_1 to T_1) and RISC (from T_1 to S_1) were estimated within the framework of Fermi's golden rule.[61,62]

$$k_{(R)ISC}^{IF} = \frac{2\pi}{\hbar} |\langle {}^1\psi_I^0 | H_{SO} | {}^3\psi_F^0 \rangle|^2 [\mathrm{FCWD}] \tag{5}$$

Here, I and F denote the initial and final excited states, FCWD represents the Franck−Condon weighted density of states, and $\langle {}^1\psi_I^0 | H_{SO} | {}^3\psi_F^0 \rangle$ defines the spin−orbit coupling. The FCWD term can be described classically in the high-temperature limit.

$$\mathrm{FCWD} = \frac{1}{\sqrt{4\pi\lambda k_B T}} \exp\left[-\frac{(\Delta E + \lambda)^2}{4\pi\lambda k_B T} \right] \tag{6}$$

Here, λ is the total reorganization energy, and ΔE is the energy difference between the initial and final states, which is ΔE_{ST} in this context, k_B is the Boltzmann constant, $\hbar$ is the reduced Planck's constant, and T is the room temperature (298 K). The transition rate between the S_1 and T_1 (vice versa) was determined by three key parameters: the spin−orbit coupling (H_{SO}), the energy difference between the two states, ΔE_{ST} (the sign is opposite for RISC and ISC), and reorganization energy λ. Large spin−orbit coupling and small coupling ($\Delta E + \lambda$) are advantageous for these processes. The total reorganization energy is the sum of the inner and outer contributions to reorganization energy. We have considered 0.2 eV as the outer reorganization energy arising from solvation effects.[61,63] The following relations were used to calculate the inner reorganization energies.

$$\lambda_{ISC} = E_{T_1/S1} - E_{T_1/T_1} \tag{7}$$

Here, E_{T_1/S_1} is the energy of the first excited triplet state in singlet geometry, and E_{T_1/T_1} is the energy of the first excited triplet state in triplet geometry. Similarly, for the RISC, we may write

$$\lambda_{RISC} = E_{S_1/T1} - E_{S_1/S_1} \tag{8}$$

Here, E_{S_1/T_1} is the energy of the first excited singlet state in triplet geometry, and E_{S_1/S_1} is the energy of the first excited singlet state in singlet geometry. The excited state geometries were used to determine the reorganization energies. Two independent methods were applied to perform single-point calculations on each geometry (singlet and triplet)—B2PLYP double-hybrid functional and wave function-based STEOM-DLPNO−CCSD, as implemented in Orca v.5.0.3. The basis sets and solvent models used were the same as those described before.

3. RESULTS AND DISCUSSION

Figure 1 displays the chemical structures of the MR-TADF complexes investigated in this study. As shown, the selected complexes cover a diverse chemical space in terms of both spectral range (400−550 nm) and different functional group compositions (BN(O), NC═O, N(O)B, N(S)B, and NS═O cores). The photophysical properties of these molecules from experimental measurements are summarized in Tables S2, S3, S7, and S10 of the Supporting Information.

3.1. ΔE_{ST} Prediction. The computed ΔE_{ST} from three different approaches are compared against the experimental measurements and are summarized in Table S2 of the Supporting Information. As evident, TD-DFT results with the TPSSh functional systematically overestimate ΔE_{ST} with a maximum deviation of around 0.3 eV (**B−O-dpAc**). However, there are a few exceptions to this observation in the case of molecules **5a**, **5b**, and **6a**, where the TD-TPSSh/6-31+G(d,p) method predicted ΔE_{ST} values are lower than those of the experiment. In emitters such as **B4** and **2c**, the TD-TPSSh estimated (0.21 and 0.39 eV) ΔE_{ST} are the closest to experimental values (0.15 and 0.31 eV). Such performance

https://doi.org/10.1021/acs.jctc.3c01147
J. Chem. Theory Comput. XXXX, XXX, XXX−XXX

of TD-DFT calculations with hybrid functional agrees with earlier reports.[31,32] It is primarily attributed to an overstabilized CT state due to a marked self-interaction error in DFT functionals. In contrast to these observations, TD-DFT computations employing a range-separated double-hybrid functional, B2PLYP, exhibit a remarkable improvement in the ΔE_{ST} prediction. Among the 37 emitters examined, only for seven of them, the TD-B2PLYP method yields a ΔE_{ST} that is ±0.1 eV different from the experiment. For most compounds, the difference between the experiment and predicted ΔE_{ST} is around ∼0.05 eV. Finally, the STEOM-DLPNO−CCSD approach shows performance on a similar level of accuracy as B2PLYP, as seen from the ΔE_{ST} values listed in Table S2 of the Supporting Information. Table 1

Table 1. MAD, RMSE, σ, and Linear Correlation Coefficient (χ^2) of S_1, T_1, and ΔE_{ST} between Experimental[12,15,16,23,47−58] and Computed Data

	TPSSh	B2PLYP	STEOM
MAD S_1 [eV]	0.098	0.224	0.275
RMSE S_1	0.165	0.263	0.330
σ S_1	0.133	0.137	0.183
χ^2 S_1	0.66	0.81	0.69
MAD T_1 [eV]	0.174	0.210	0.230
RMSE T_1	0.198	0.250	0.280
σ T_1	0.095	0.139	0.157
χ^2 T_1	0.71	0.71	0.67
MAD ΔE_{ST} [eV]	0.201	0.056	0.061
RMSE ΔE_{ST}	0.210	0.076	0.088
σ ΔE_{ST}	0.06	0.051	0.063
χ^2 ΔE_{ST}	0.25	0.85	0.79

summarizes the MAD, RMSE, σ, and linear correlation coefficient (χ^2) between the experiment and the computed data to assess the accuracy of these methods. It is apparent from Table 1 that TD-TPSSh calculations exhibit a MAD of 0.20 eV for these molecules, which is much larger than that of TD-B2PLYP or STEOM-DLPNO−CCSD calculations. It is interesting to note that the TPSSh functional yields much smaller MAD when compared to other DFT functionals, including the long-range corrected functionals such as CAM-B3LYP or LC-ωPBE, as reported by Hall et al.[31] A remarkable improvement in the MAD for predicted ΔE_{ST} is observed, around 0.06 eV, when either TD-B2PLYP or STEOM-DLPNO−CCSD methods are utilized. Both STEOM-DLPNO−CCSD and TD-B2PLYP yield very similar RMSE and σ values as listed in Table 1, implying their close agreement in ΔE_{ST} prediction. Such enhanced performance demonstrates the importance and role of improved electron correlation descriptions owing to the (partial) inclusion of double excitations. This is even more apparent since the double hybrid functional only accounts for the double excitations for the excited singlet states, which produces a MAD as good as that of the STEOM-DLPNO−CCSD method. Moreover, the STEOM-DLPNO−CCSD or TD-B2PLYP computed MAD (0.06 eV) is close to the one obtained from the SCS-CC2 method (0.04 eV) as reported by Hall et al.[31]

Figure 2 displays the correlation between the experiment and the predicted vertical ΔE_{ST} gathered from three different strategies. When all of the data points are included in the analysis, we observe a correlation coefficient of χ^2 = 0.70 from

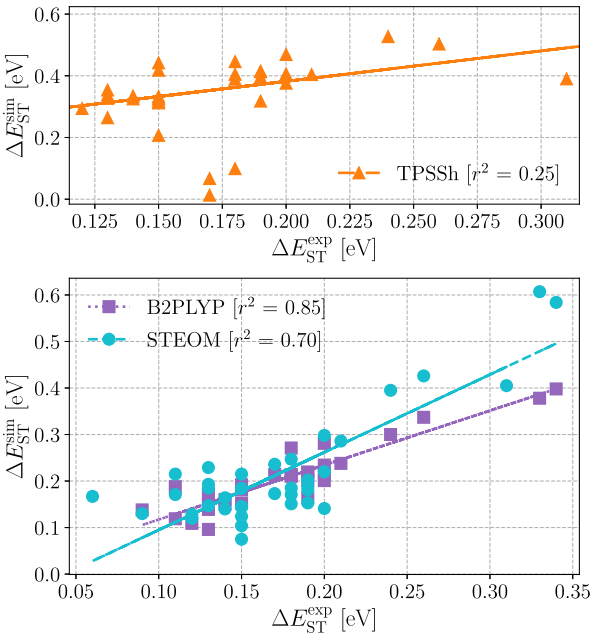

Figure 2. Experimental versus predicted vertical ΔE_{ST} using three different theoretical approaches—TD-TPSSh, TD-B2PLYP, and STEOM-DLPNO−CCSD. The straight lines represent the linear fit of the data procured at each level of theory.

the STEOM-DLPNO−CCSD method. However, χ^2 improves to 0.79 when we include only those emitters (14 out of a total of 37) for which STEOM-DLPNO−CCSD predicted ΔE_{ST} is within ±0.026 eV compared to the experiment. On the other hand, the double-hybrid functional B2PLYP yields a much poorer χ^2 of 0.32 considering the entire data points. Remarkably, χ^2 improves to 0.85 when we include only those complexes (30 out of a total of 37) for which TD-B2PLYP predicted ΔE_{ST} is within ±0.1 eV compared to the experiment. As is evident from Table S2 of the Supporting Information, the TD-B2PLYP approach can produce an improved χ^2 value for a more extensive set of compounds than that of the STEOM-DLPNO−CCSD method. This observation clearly demonstrates the accuracy of the TD-B2PLYP method in predicting ΔE_{ST} comparable to STEOM-DLPNO−CCSD or earlier reported SCS-CC2 computed results by Hall et al.[31] Given the fact that the B2PLYP method only accounts for double excitation for the excited singlet states and requires a minimal computation time compared to wave function-based calculation, these observations are very promising and portray the applicability of TD-B2PLYP as the least computationally demanding method for future modeling of MR-TADF complexes. Finally, the lowest χ^2 value (0.25) is observed for the standard TPSSh functional.

3.2. Excited-State Energies. The future design and development of MR-TADF type emitter materials rely on computational methodologies that can accurately predict ΔE_{ST} and, simultaneously, the absolute energies of both S_1 and T_1 energies. The computed S_1 and T_1 energies are collected and compared against the experimental results in Table S3 of the Supporting Information. Figure 3 illustrates the correlation between the experimental and predicted vertical excitation energies (S_1 and T_1) computed using three different methods. The computation of vertical excitation energies using the ground state optimized geometries as an approximation to the lowest-lying excited state energies is justified due to the small

https://doi.org/10.1021/acs.jctc.3c01147
J. Chem. Theory Comput. XXXX, XXX, XXX−XXX

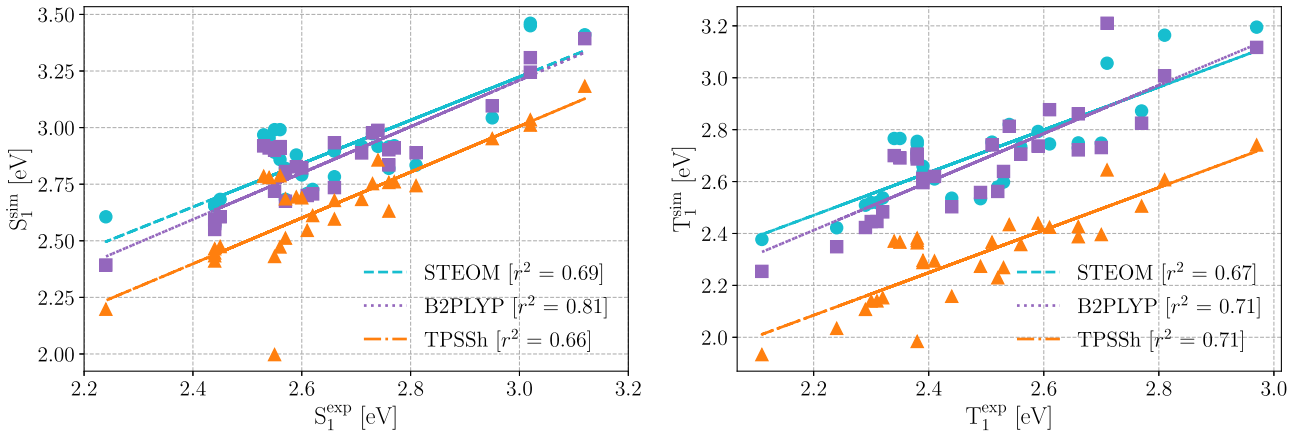

Figure 3. Experimental S_1 and T_1 vs predicted vertical excitation energies of each emitter using three different theoretical approaches—TD-TPSSh, TD-B2PLYP, and STEOM-DLPNO−CCSD. The straight lines represent the linear fit of the data procured at each level of theory.

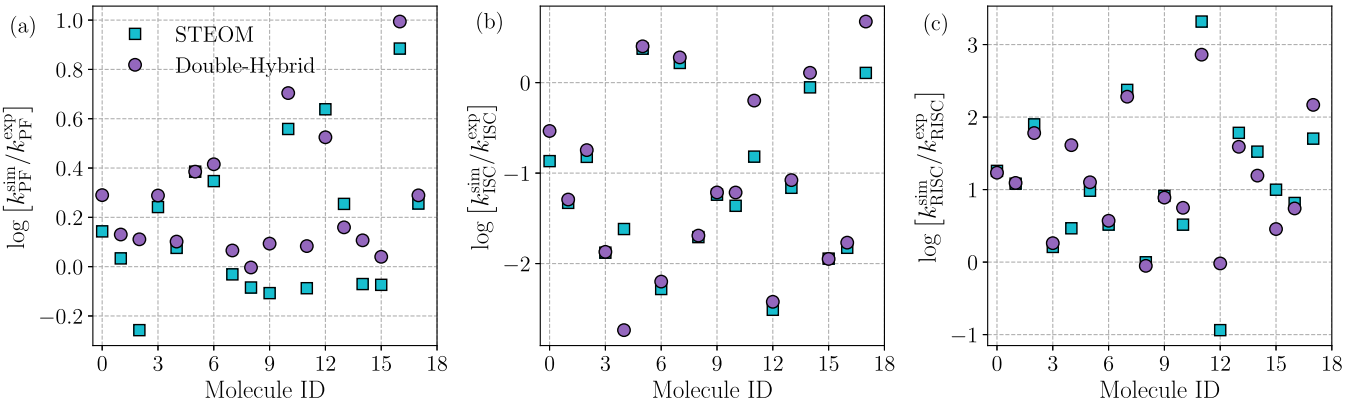

Figure 4. Experimental versus predicted rate constants of k_{PF}, k_{ISC}, and k_{RISC}—obtained using STEOM-DLPNO−CCSD and double-hybrid (TD-B2PLYP) approaches across different emitters investigated in this study.

Stokes observed owing to the rigid structures of the MR-TADF complexes. As seen from Table 1, the TD-TPSSh approach yields the minimum MAD of 0.098 eV for the S_1 energy compared to TD-B2PLYP (0.224 eV) or even STEOM-DLPNO−CCSD (0.275 eV). A similar order in MAD is followed in the case of T_1 energy; however, the MAD for T_1 energy (0.17 eV) from the TD-TPSSh method is almost double as compared to the MAD for S_1 energy. Whereas both TD-B2PLYP and STEOM-DLPNO−CCSD approaches produce T_1 MAD values (0.21 and 0.23 eV) in the same order as the S_1 MAD (0.224 and 0.275 eV). This is why the remarkably small ΔE_{ST} is observed from the latter methods. We compared our results to that of SCS-CC2 outcomes as reported in ref 31. The MAD for S_1 and T_1 obtained using the SCS-CC2 method was reported to be 0.55 and 0.56 eV, much larger than our results obtained from any of these three approaches. Considering the diverse nature of emitters examined, the presence of such small MAD values is a testament to the accuracy of the TD-B2PLYP and STEOM-DLPNO−CCSD methods employed in this study. Figure 3 shows a remarkable linear correlation (χ^2 = 0.81) between the experimental and TD-B2PLYP computed S_1 energies. Similar correlation coefficients obtained via STEOM-DLPNO−CCSD (0.69) and TD-TPSSh (0.66) methods are smaller in magnitude. However, in the case of T_1 energies, the magnitude of χ^2 is reduced to 0.71 at the TD-B2PLYP level of theory whereas for the STEOM-DLPNO−CCSD (0.67) and TD-TPSSh (0.71) methods yield χ^2 in a similar order as seen for S_1 energies. Such a reduction in the χ^2 value when TD-B2PLYP is utilized can be attributed to the lack of electron correlation due to the absence of double excitation information for the triplet excited states within the double-hybrid functionals. These quantitative comparisons once again ascertain the efficacy of the TD-B2PLYP technique in predicting excited state energies at par with wave function-based simulations, but of course, at much lower computational expenses. In the following sections, we describe the radiative/nonradiative rates and exciton characteristics, whereby we provide a comparison between TD-B2PLYP and STEOM-DLPNO−CCSD results with the available experimental measurements. The TD-TPSSh method is not included thus far since it lacks the accuracy to describe ΔE_{ST}, which is one of the critical parameters in governing the radiative rates.

3.3. Reorganization Energy. Figure S1 of the Supporting Information displays the correlation between reorganization energies associated with ISC and RISC processes computed using two different approaches—STEOM-DLPNO−CCSD and TD-B2PLYP. We have also included the ΔE_{ST} comparison between these two methods in Figure S1a for completeness. It is important to note that this analysis includes only those emitters for which experiential rates of radiative/nonradiative processes are available. This is primarily because we aim to compare those experimental rates against the computed rates in the following section. The computed reorganization energies

https://doi.org/10.1021/acs.jctc.3c01147
J. Chem. Theory Comput. XXXX, XXX, XXX−XXX

considering internal and outer-sphere contributions are tabulated in Tables S5 and S6 of the Supporting Information. Similar to our previous observation, it is apparent from Figure S1a that there is a strong agreement between STEOM-DLPNO−CCSD and TD-B2PLYP methods while predicting the ΔE_{ST} in these MR-TADF emitters, as both procedures yield a MAD of 0.06 eV (see Table 1). As seen from Figure S1b, TD-B2PLYP predicted reorganization energies involving RISC events correlate satisfactorily with STEOM-DLPNO−CCSD calculations. Contrary to this, reorganization energies for the ISC processes do not compare well between these two methods, as shown in Figure S1c. It is to be noted here that the reorganization energies were evaluated using eqs 7 and 8. It is evident in the formulation that while the organization energies for the RISC process depend on the excited singlet state energies (at two different geometries), the similar quantity for the counterpart (ISC events) are determined by the excited triplet state energies (at two different geometries). Since the double-hybrid functional B2PLYP only accommodates double excitation information for the excited singlet state, it can describe the S_1 energies in close agreement with STEOM-DLPNO−CCSD computed values. At the same time, it deviates from the STEOM-DLPNO−CCSD results when it comes to the T_1 energies.

3.4. Radiative and Nonradiative Rates. The rates of different processes, k_{PF}, k_{ISC}, and k_{RISC} were estimated using eqs 4 and 5. The evaluated rate constants via STEOM-DLPNO−CCSD and TD-B2PLYP methods are collected and compared against the experimental measurements in Table S7 of the Supporting Information. Figure 4 displays the logarithmic ratio of the rate constants between experimental and computed values for a few MR-TADF emitters. Thus, an ideal agreement would yield a magnitude of the ratio of around zero on the *y*-axis. The blue squares and purple circles represent STEOM-DLPNO−CCSD and TD-B2PLYP results, respectively. Figure 4a illustrates a comparison for fluorescence rate constants. It is evident that there is an excellent agreement between predicted and experimental fluorescence rates across all the emitters, as shown by the log of ratio to be less than ±1. The maximum deviation observed is less than an order of magnitude for both STEOM-DLPNO−CCSD and TD-B2PLYP approaches. The double-hybrid procedure consistently exhibits a slightly larger magnitude of k_{PF} compared to that of STEOM-DLPNO−CCSD predictions. On the other hand, the rates of ISC and RISC events are compared in Figure 4b,c. It is apparent that for both k_{ISC} and k_{RISC}, the deviations are larger for both methods compared to k_{PF}. In general, while the rate constants of ISC are underestimated, the RISC rates are overestimated by almost a similar magnitude. Except for three molecules, the differences in k_{ISC} and k_{RISC} between experimental measurements and predictions from both approaches fall within 2 orders of magnitude. Such a quantitative difference of 2 orders of magnitude between the experiment and computed k_{ISC} rates using the STEOM-DLPNO−CCSD method was earlier reported by Brédas and co-workers in MR-TADF complexes.[37] This discrepancy could be attributed to the description of excited state energies and the determination of spin−orbit coupling based on ground-state geometries rather than the true adiabatic potential energy surfaces. Nevertheless, what is most important here is that the differences observed are consistent across the examined emitters, and the trend in the rate constants compares well with the order in experimental values. Thus, the two approaches presented here can provide physically meaningful rates of fluorescence, ISC, and RISC events that can be used in future modeling of MR-TADF emitters. It is worth mentioning that the TD-B2PLYP procedure provides an almost similar level of accuracy as compared to the wave function-based STEOM-DLPNO−CCSD method at a much reduced computational overhead.

The above rate constants consider only the transitions involving $S_1 \leftrightarrow T_1$. Dias et al. demonstrated that coupling between various triplet states facilitates the TADF mechanism, with an intermediate triplet state playing a crucial role.[64] The TADF mechanism via the mediated triplet state is attributed to vibrational frequency resonance in MR-TADFs, elucidated in recent work by Kim et al.[65] They expound on the role of an intermediate state in the ISC and RISC mechanism and showed that in MR-TADF compounds the S_1,T_1,T_3 states play an analogous role to $CT^1/CT^3/LE^3$ in the D−A type TADF system. Drummond et al. illustrated that high-lying triplet excitons, which were initially nonaccessible, can be made accessible and involved in the mechanism under specific energy conditions, spin−orbit coupling, and the nature of interacting states.[66] Moreover, Elsayed's rule asserts that for effective interaction between singlet and triplet states, they should possess different characters—if one is of charge transfer (CT) type, the other should be locally excited (LE) type. The transitions between states of the same type (CT−CT or LE−LE) must be mediated via LE and CT states, respectively. Another investigation involving *ν*-DABNA molecule revealed the coupling between T_1 and T_2 states and the mechanism of RISC via the T_2 state.[67] Furthermore, Northey and Penfold discussed the nature of the intermediate T_2 state. They obtained a sizable singlet−triplet energy gap between the first singlet and triplet states, with reduced spin−orbit coupling (SOC) compared to the energy gap and SOC obtained from S_1 and T_2 state. Consequently, the intermediate state was identified as T_2.[68] Therefore, we investigated the role of higher-lying triplet states in ISC and RISC events in these MR-TADF emitters. Accordingly, these rates were evaluated using STEOM-DLPNO−CCSD and TD-B2PLYP procedures considering $S_1 \leftrightarrow T_2$ transitions and are summarized in Table S8 of the Supporting Information. To discern the role of T_2 states in the TADF mechanism, we first compare the relative positions of T_1 and T_2 states with respect to S_1 state. Figure 5 displays the S_1-T_1 and S_1-T_2 energy differences in the selected MR-TADF complexes in this study. As evident from Figure 5, both methods generally exhibit a T_2 state at much higher energy relative to the S_1 state in these studied emitters. Since the T_2 state lies above the S_1 state, the energetically downhill RISC process becomes highly favorable as opposed to the uphill ISC counterpart. Consequently, the RISC rate constants computed involving $T_2 \leftrightarrow S_1$ transitions are significantly higher than that of $S_1 \leftrightarrow T_2$ ISC transitions. The magnitudes of these rates are tabulated in Table S8 of the Supporting Information. As can be seen, the much higher (lowered) RISC (ISC) rate constants are unphysical when compared to the available experimental measurements. These observations thus conclude that the TADF mechanism in these MR-TADF complexes is primarily due to transitions involving S_1 and T_1 states, corresponding to results reported in the ref 31.

3.5. Exciton Characteristics. One of the critical signatures of MR-TADF-based emitters that separates them from their regular TADF counterpart is the nature of excitons, primarily

https://doi.org/10.1021/acs.jctc.3c01147
J. Chem. Theory Comput. XXXX, XXX, XXX−XXX

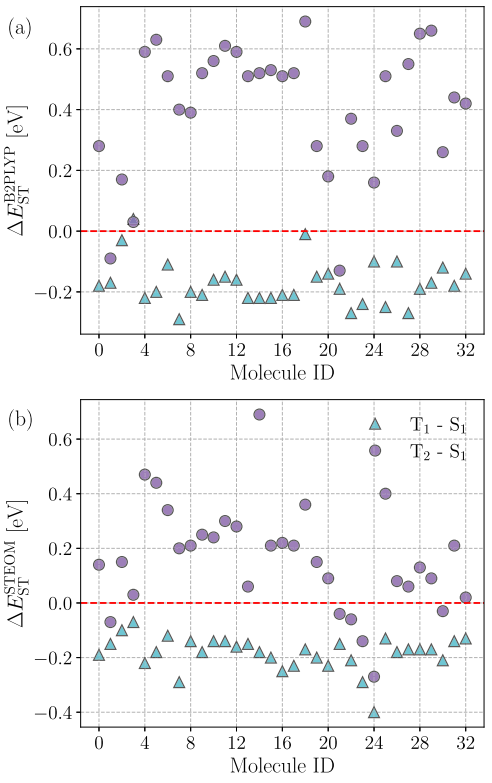

Figure 5. Relative positions of T_1 (cyan-triangle) and T_2 (purple-circle) states with respect to the S_1 (red-colored dotted line) state in the investigated MR-TADF complexes: (a) TD-B2PLYP and (b) STEOM-DLPNO−CCSD.

of short-range or local charge transfer (SRCT) character promoted by the MR effect. Such hallmarks of MR-TADF emitters represented by SRCT excited states are often accessed by analyzing density difference plots. An accurate and reliable design of future MR-TADF complexes driven by a computational approach thus depends on a particular method's ability to adequately describe the nature of excited states in these exotic materials. The difference density plots (Δ) were obtained using the following relation: $\Delta = \rho_{ex} - \rho_0$. Here, ρ_{ex} and ρ_0 represent the excited-state (S_1) and ground-state densities, respectively. In addition to Δ, we have evaluated an important descriptor, the overlap integral ($S_{\pm}$), for quantitative assessment of exciton characteristics. $S_{\pm}$ accounts for the overlap between ρ_+ and ρ_- (increased and decreased electron density)—an overlap of 1 suggests an SRCT (LE) state, while a value of 0 resembles a CT state. These calculations were based on the difference density plots employing the Multiwfn program.[69] The density difference plots were generated using the VESTA software package.[70] The computed $S_{\pm}$ values are summarized in Table S9 of the Supporting Information.

Figure 6 displays the computed difference density plots by using the STEOM-DLPNO−CCSD method for the selected MR-TADF emitters in this study. For the remaining molecules, the density difference patterns are shown in Figure S3 of the Supporting Information. A similar plot obtained utilizing the TD-B2PLYP approach is shown in Figure S4 of the Supporting Information. As seen from Figures 6 and S3−S4, the decreased and increased density represented by blue and yellow lobes, respectively, are localized on adjacent atoms—thereby confirming the SRCT nature of these MR-TADF emitters as assigned experimentally. Similar patterns were also confirmed by Hall et al. employing the SCS-CC2 method.[31] To further confirm the SRCT character of the excited states, we analyze the $S_{\pm}$ values as tabulated in Table S9 of the Supporting Information. It is apparent from Table S9 that all molecules, except for **6a**, possess an $S_{\pm}$ close to 1, implying a strong short-range nature of the excited state. Another hallmark of MR-TADF type emitters is the presence of narrow full width at half-maximum (fwhm) values. The computed fwhm employing STEOM-DLPNO−CCSD and TD-B2LYP methods are collected and compared against the available experimental measurements in Table S10 of the Supporting Information. As can be seen, the predicted fwhm resembles an experiment

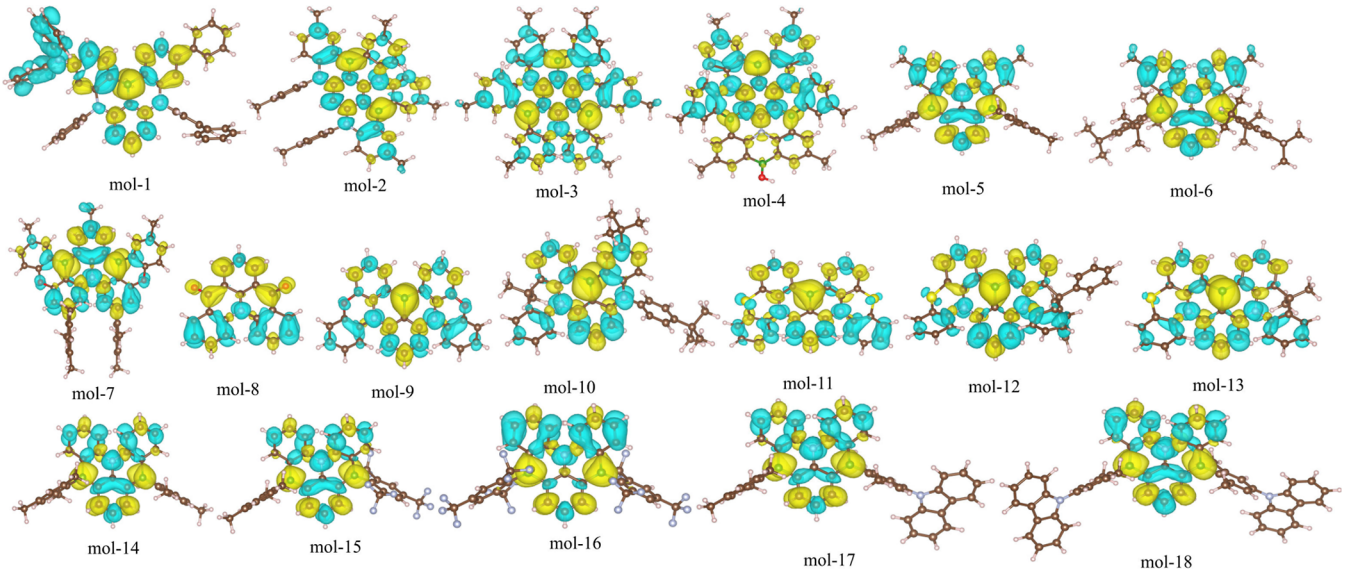

Figure 6. Difference density patterns calculated using the STEOM-DLPNO−CCSD method for the emitter molecules for the first singlet excited state (S_1), where blue and yellow lobes represent decreased and increased density, respectively (isovalue = 0.001). Density difference plots of the remaining compounds are shown in Figure S3 of the Supporting Information. Similar patterns computed using the TD-B2PLYP approach are shown in Figure S4 of the Supporting Information.

https://doi.org/10.1021/acs.jctc.3c01147
J. Chem. Theory Comput. XXXX, XXX, XXX−XXX

within a maximum deviation of around 10 nm. Strong agreement between the experiment and computed results via the two approaches is indeed encouraging and shows the robustness of the employed strategies. An essential outcome of these analyses is the accuracy of the double-hybrid functional, B2PLYP, in determining exciton characteristics. It is not surprising to see the ability of a wave function-based approach, STEOM-DLPNO−CCSD, to capture such critical aspects of MR-TADF emitters. However, the capacity of the double-hybrid functional within the TD-DFT framework should be considered a crucial finding of this study. The significance is more since TD-B2PLYP can deliver such accuracy while considering double excitation information only for the excited singlet states. More importantly, performing TD-B2PLYP computations is not as CPU-intensive as the wave function-based methods, helping reduce the overall computational overhead.

4. CONCLUSIONS

We investigated MR-TADF emitters employing hybrid and range-separated double-hybrid functionals within the TD-DFT framework and the wave function-based STEOM-DLPNO−CCSD method to establish an accurate and cost-effective methodology for the prediction of ΔE_{ST}, rate constants of radiative and nonradiative events, and the nature of excited states in these exotic materials. We demonstrated the importance of including double excitations while predicting the correct excited state energies and ΔE_{ST}, an observation well documented in earlier reports.[31,32] Reaffirming previous studies, we showed that the hybrid density functional (TPSSh) within the TD-DFT framework fails drastically to capture the correct description of excited state energies due to its inability to account for Coulomb electron correlations accurately. Our findings illustrated the robustness of STEOM-DLPNO−CCSD and TD-B2PLYP approaches in predicting ΔE_{ST}, as quantified by a significantly small MAD of 0.06 eV across 37 emitters. The accuracy of these methods is at par with earlier reported MAD of 0.04 eV associated with ΔE_{ST} prediction in MR-TADF complexes by Hall et al.[31] In addition to ΔE_{ST}, the double-hybrid B2PLYP and STEOM-DLPNO−CCSD predicted MAD for excited singlet and triplet state energies are around ∼0.2 eV, much smaller than SCS-CC2 predicted MAD for the exact quantities reported in ref 31. These quantitative comparisons, obtained from a chemically diverse set of MR-TADF complexes, evidently depict the transferability and applicability of the two approaches investigated in this study. It is, therefore, highly recommended that a computational methodology described here that incorporates (partial) double excitations to examine and design MR-TADF materials in the future. Apart from an accurate prediction of excited state energies and ΔE_{ST}, both TD-B2PLYP and STEOM-DLPNO−CCSD methods demonstrated the capacity to capture the short-range (local charge transfer) charge transfer nature of the low-lying excited states, a hallmark of this particular class of emitters.

We further examined the rate constants of radiative and nonradiative events and their associated elements via TD-B2PLYP and STEOM-DLPNO−CCSD approaches. While the predicted k_{PF} using these methods display excellent agreement with experimental rate constants (Figure 4a) across all the emitters, the computed k_{ISC} and k_{RISC} show deviation of around 2 orders of magnitude compared to experimental observations. It is worth mentioning that such differences were also observed in earlier reports employing STEOM-DLPNO−CCSD theory by Bredas and co-workers.[37,38] Such a discrepancy could be attributed to the description of excited state energies and spin−orbit coupling based on ground-state geometries rather than the actual adiabatic potential energy surfaces. Nevertheless, the predicted trend in the rate constants follows the order in the experimental measurements. We also characterized the higher-lying triplet (T_2) excited states in these complexes to confirm whether those states contribute to the RISC mechanism. We found via both methods that in most cases, these states are located at much higher energy, producing unphysically increased magnitudes of RISC rates compared to the experiment, thus confirming their absence in the TADF mechanism in these studied MR-TADF complexes. These critical observations and the quantitative estimation of energies and rates with available experimental data testify to the strength of the two computational approaches described here, precisely their versatility, transferability, and robustness in capturing the correct (excited state) chemistry. It is often seen that primarily due to the computational overhead of wave function-based methods, the community tends to adopt the single-excitation TD-DFT methods to describe the excited states of MR-TADF complexes even though such TD-DFT formalism fails to predict both energies and the nature of excited states in these complexes. Methodologies presented in this work will be helpful to the community, as it opens up a new computationally cost-effective avenue for accurate design and development of MR-TADF emitters for future light-emitting applications.

■ ASSOCIATED CONTENT

Supporting Information

The Supporting Information is available free of charge at https://pubs.acs.org/doi/10.1021/acs.jctc.3c01147.

Mapping of investigated molecules in the present work with the names used in experimental work; experimental and computed singlet-triplet (S_1-T_1) energy differences (eV) for the investigated MR-TADF emitters; computed values (eV) of excited single-state (S_1) and triplet-state (T_1) energies at different levels of theory and their comparison against experimental results; comparison of oscillator strength corresponding to the transition between $S_1 \rightarrow S_0$ and $S_2 \rightarrow S_0$ with the TD-DFT and STEOM-DLPNO-CCSD methods; TD-B2PLYP computed singlet and triplet energies (eV) in singlet and triplet geometries and the associated reorganization energies for ISC and RISC events in the examined MR-TADF complexes; STEOM-DLPNO-CCSD computed singlet and triplet energies (eV) in singlet and triplet geometries and the associated reorganization energies for ISC and RISC events in the examined MR-TADF complexes; STEOM-DLPNO-CCSD and TD-B2PLYP computed rate constants — k_{PF} ($\times 10^8$ s^{-1}), k_{ISC} ($\times 10^7$ s^{-1}), and k_{RISC} ($\times 10^4$ s^{-1}) considering S_1-T_1 transitions, compared against available experimental measurements; STEOM-DLPNO-CCSD and TD-B2PLYP computed rate constants — k_{ISC} ($\times 10^5$ s^{-1}) and k_{RISC} ($\times 10^7$ s^{-1}) considering S_1-T_2 transitions; computed overlap integral ($S_\pm$) values in the investigated MR-TADF emitters for quantitatively estimating CT or SRCT character of the excited states; STEOM-DLPNO-CCSD and TD-B2PLYP computed full width at half maximum (in

https://doi.org/10.1021/acs.jctc.3c01147
J. Chem. Theory Comput. XXXX, XXX, XXX−XXX

nm) compared against the experimental results; comparison between predicted ΔE_{ST} and reorganization energies (ISC and RISC) obtained using STEOM-DLPNO-CCSD and double-hybrid (TD-B2PLYP) approaches; correlation between STEOM-DLPNO-CCSD and TD-DFT (TPSSh and B2PLYP) computed oscillator strengths in the investigated MR-TADF emitters; difference density patterns calculated using STEOM-DLPNO-CCSD method for the emitter molecules for the first singlet excited state (S_1); and difference density patterns calculated using TD-B2PLYP method for the emitter molecules for the first singlet excited state (S_1) (PDF)

AUTHOR INFORMATION

Corresponding Author

Anirban Mondal − *Department of Chemistry, Indian Institute of Technology Gandhinagar, Gandhinagar, Gujarat 382355, India;* orcid.org/0000-0003-3029-8840; Email: amondal@iitgn.ac.in

Authors

Sanyam − *Department of Chemistry, Indian Institute of Technology Gandhinagar, Gandhinagar, Gujarat 382355, India;* orcid.org/0000-0001-7410-8207

Rudranarayan Khatua − *Department of Chemistry, Indian Institute of Technology Gandhinagar, Gandhinagar, Gujarat 382355, India*

Complete contact information is available at: https://pubs.acs.org/10.1021/acs.jctc.3c01147

Notes

The authors declare no competing financial interest.

ACKNOWLEDGMENTS

The authors gratefully acknowledge the Indian Institute of Technology, Gandhinagar, India, for providing research facilities and financial support. Sanyam thanks CSIR for the fellowship. A.M. acknowledges the SERB (SRG/2022/001532) project for funding. We thank PARAM Ananta for computational resources.

REFERENCES

(1) Endo, A.; Sato, K.; Yoshimura, K.; Kai, T.; Kawada, A.; Miyazaki, H.; Adachi, C. Efficient up-conversion of triplet excitons into a singlet state and its application for organic light emitting diodes. *Appl. Phys. Lett.* **2011**, *98*, 083302.

(2) Uoyama, H.; Goushi, K.; Shizu, K.; Nomura, H.; Adachi, C. Highly efficient organic light-emitting diodes from delayed fluorescence. *Nature* **2012**, *492*, 234−238.

(3) Liu, Y.; Li, C.; Ren, Z.; Yan, S.; Bryce, M. R. All-organic thermally activated delayed fluorescence materials for organic light-emitting diodes. *Nat. Rev. Mater.* **2018**, *3*, 18020.

(4) Xu, Y.; Cheng, Z.; Li, Z.; Liang, B.; Wang, J.; Wei, J.; Zhang, Z.; Wang, Y. Molecular-structure and device-configuration optimizations toward highly efficient green electroluminescence with narrowband emission and high color purity. *Adv. Opt. Mater.* **2020**, *8*, 1902142.

(5) Xu, Y.; Li, C.; Li, Z.; Wang, Q.; Cai, X.; Wei, J.; Wang, Y. Constructing Charge-Transfer Excited States Based on Frontier Molecular Orbital Engineering: Narrowband Green Electroluminescence with High Color Purity and Efficiency. *Angew. Chem.* **2020**, *132*, 17595.

(6) Izumi, S.; Higginbotham, H. F.; Nyga, A.; Stachelek, P.; Tohnai, N.; Silva, P. d.; Data, P.; Takeda, Y.; Minakata, S. Thermally activated delayed fluorescent donor−acceptor−donor−acceptor π-conjugated macrocycle for organic light-emitting diodes. *J. Am. Chem. Soc.* **2020**, *142*, 1482−1491.

(7) Goushi, K.; Yoshida, K.; Sato, K.; Adachi, C. Organic light-emitting diodes employing efficient reverse intersystem crossing for triplet-to-singlet state conversion. *Nat. Photonics* **2012**, *6*, 253−258.

(8) Stachelek, P.; Ward, J. S.; dos Santos, P. L.; Danos, A.; Colella, M.; Haase, N.; Raynes, S. J.; Batsanov, A. S.; Bryce, M. R.; Monkman, A. P. Molecular Design Strategies for Color Tuning of Blue TADF Emitters. *ACS Appl. Mater. Interfaces* **2019**, *11*, 27125−27133.

(9) Cao, X.; Zhang, D.; Zhang, S.; Tao, Y.; Huang, W. CN-Containing donor−acceptor-type small-molecule materials for thermally activated delayed fluorescence OLEDs. *J. Mater. Chem. C* **2017**, *5*, 7699−7714.

(10) Ha, J. M.; Hur, S. H.; Pathak, A.; Jeong, J.-E.; Woo, H. Y. Recent advances in organic luminescent materials with narrowband emission. *NPG Asia Mater.* **2021**, *13*, 53.

(11) Zhang, Y.; Zhang, D.; Wei, J.; Hong, X.; Lu, Y.; Hu, D.; Li, G.; Liu, Z.; Chen, Y.; Duan, L. Achieving pure green electroluminescence with CIEy of 0.69 and EQE of 28.2% from an aza-fused multi-resonance emitter. *Angew. Chem.* **2020**, *132*, 17652−17656.

(12) Oda, S.; Kawakami, B.; Kawasumi, R.; Okita, R.; Hatakeyama, T. Multiple resonance effect-induced sky-blue thermally activated delayed fluorescence with a narrow emission band. *Org. Lett.* **2019**, *21*, 9311−9314.

(13) Han, S. H.; Jeong, J. H.; Yoo, J. W.; Lee, J. Y. Ideal blue thermally activated delayed fluorescence emission assisted by a thermally activated delayed fluorescence assistant dopant through a fast reverse intersystem crossing mediated cascade energy transfer process. *J. Mater. Chem. C* **2019**, *7*, 3082−3089.

(14) Pershin, A.; Hall, D.; Lemaur, V.; Sancho-Garcia, J.-C.; Muccioli, L.; Zysman-Colman, E.; Beljonne, D.; Olivier, Y. Highly emissive excitons with reduced exchange energy in thermally activated delayed fluorescent molecules. *Nat. Commun.* **2019**, *10*, 597.

(15) Matsui, K.; Oda, S.; Yoshiura, K.; Nakajima, K.; Yasuda, N.; Hatakeyama, T. One-shot multiple borylation toward BN-doped nanographenes. *J. Am. Chem. Soc.* **2018**, *140*, 1195−1198.

(16) Yang, M.; Park, I. S.; Yasuda, T. Full-Color, Narrowband, and High-Efficiency Electroluminescence from Boron and Carbazole Embedded Polycyclic Heteroaromatics. *J. Am. Chem. Soc.* **2020**, *142*, 19468−19472.

(17) Hall, D.; Suresh, S. M.; dos Santos, P. L.; Duda, E.; Bagnich, S.; Pershin, A.; Rajamalli, P.; Cordes, D. B.; Slawin, A. M. Z.; Beljonne, D.; et al. Improving Processability and Efficiency of Resonant TADF Emitters: A Design Strategy. *Adv. Opt. Mater.* **2020**, *8*, 1901627.

(18) Qiu, X.; Tian, G.; Lin, C.; Pan, Y.; Ye, X.; Wang, B.; Ma, D.; Hu, D.; Luo, Y.; Ma, Y. Narrowband Emission from Organic Fluorescent Emitters with Dominant Low-Frequency Vibronic Coupling. *Adv. Opt. Mater.* **2021**, *9*, 2001845.

(19) Lee, Y.-T.; Chan, C.-Y.; Tanaka, M.; Mamada, M.; Balijapalli, U.; Tsuchiya, Y.; Nakanotani, H.; Hatakeyama, T.; Adachi, C. Investigating HOMO Energy Levels of Terminal Emitters for Realizing High-Brightness and Stable TADF-Assisted Fluorescence Organic Light-Emitting Diodes. *Adv. Electron. Mater.* **2021**, *7*, 2001090.

(20) Huang, F.; Wang, K.; Shi, Y.-Z.; Fan, X.-C.; Zhang, X.; Yu, J.; Lee, C.-S.; Zhang, X.-H. Approaching Efficient and Narrow RGB Electroluminescence from D−A-Type TADF Emitters Containing an Identical Multiple Resonance Backbone as the Acceptor. *ACS Appl. Mater. Interfaces* **2021**, *13*, 36089−36097.

(21) Zhang, Y.; Zhang, D.; Wei, J.; Liu, Z.; Lu, Y.; Duan, L. Multi-resonance induced thermally activated delayed fluorophores for narrowband green OLEDs. *Angew. Chem., Int. Ed. Engl.* **2019**, *58*, 16912−16917.

(22) Oda, S.; Sugitani, T.; Tanaka, H.; Tabata, K.; Kawasumi, R.; Hatakeyama, T. Development of Pure Green Thermally Activated Delayed Fluorescence Material by Cyano Substitution. *Adv. Mater.* **2022**, *34*, 2201778.

(23) Park, J.; Lim, J.; Lee, J. H.; Jang, B.; Han, J. H.; Yoon, S. S.; Lee, J. Y. Asymmetric Blue Multiresonance TADF Emitters with a Narrow Emission Band. *ACS Appl. Mater. Interfaces* **2021**, *13*, 45798−45805.
(24) Samanta, P. K.; Kim, D.; Coropceanu, V.; Brédas, J. L. Up-Conversion Intersystem Crossing Rates in Organic Emitters for Thermally Activated Delayed Fluorescence: Impact of the Nature of Singlet vs Triplet Excited States. *J. Am. Chem. Soc.* **2017**, *139*, 4042−4051.
(25) Bas, E. E.; Ulukan, P.; Monari, A.; Aviyente, V.; Catak, S. Photophysical properties of benzophenone-based TADF emitters in relation to their molecular structure. *J. Phys. Chem. A* **2022**, *126*, 473−484.
(26) Becke, A. D. A new mixing of Hartree−Fock and local density-functional theories. *J. Chem. Phys.* **1993**, *98*, 1372−1377.
(27) Adamo, C.; Barone, V. Toward reliable density functional methods without adjustable parameters: The PBE0 model. *J. Chem. Phys.* **1999**, *110*, 6158−6170.
(28) Zhao, Y.; Truhlar, D. G. The M06 suite of density functionals for main group thermochemistry, thermochemical kinetics, noncovalent interactions, excited states, and transition elements: two new functionals and systematic testing of four M06-class functionals and 12 other functionals. *Theor. Chem. Acc.* **2008**, *120*, 215−241.
(29) Vydrov, O. A.; Scuseria, G. E. Assessment of a long-range corrected hybrid functional. *J. Chem. Phys.* **2006**, *125*, 234109.
(30) Yanai, T.; Tew, D. P.; Handy, N. C. A new hybrid exchange−correlation functional using the Coulomb-attenuating method (CAM-B3LYP). *Chem. Phys. Lett.* **2004**, *393*, 51−57.
(31) Hall, D.; Sancho-García, J. C.; Pershin, A.; Beljonne, D.; Zysman-Colman, E.; Olivier, Y. Benchmarking DFT Functionals for Excited-State Calculations of Donor−Acceptor TADF Emitters: Insights on the Key Parameters Determining Reverse Inter-System Crossing. *J. Phys. Chem. A* **2023**, *127*, 4743−4757.
(32) Hall, D.; Sancho-García, J. C.; Pershin, A.; Ricci, G.; Beljonne, D.; Zysman-Colman, E.; Olivier, Y. Modeling of Multiresonant Thermally Activated Delayed Fluorescence Emitters-Properly Accounting for Electron Correlation Is Key. *J. Chem. Theory Comput.* **2022**, *18*, 4903−4918.
(33) Ghosh, S.; Bhattacharyya, K. Origin of the failure of density functional theories in predicting inverted singlet−triplet gaps. *J. Phys. Chem. A* **2022**, *126*, 1378−1385.
(34) Shizu, K.; Kaji, H. Comprehensive understanding of multiple resonance thermally activated delayed fluorescence through quantum chemistry calculations. *Commun. Chem.* **2022**, *5*, 53.
(35) Hatakeyama, T.; Shiren, K.; Nakajima, K.; Nomura, S.; Nakatsuka, S.; Kinoshita, K.; Ni, J.; Ono, Y.; Ikuta, T. Ultrapure blue thermally activated delayed fluorescence molecules: efficient HOMO−LUMO separation by the multiple resonance effect. *Adv. Mater.* **2016**, *28*, 2777−2781.
(36) Tajti, A.; Kozma, B.; Szalay, P. G. Improved description of charge-transfer potential energy surfaces via spin-component-scaled CC2 and ADC (2) methods. *J. Chem. Theory Comput.* **2021**, *17*, 439−449.
(37) Pratik, S. M.; Coropceanu, V.; Brédas, J. L. Purely organic emitters for multiresonant thermally activated delay fluorescence: design of highly efficient sulfur and selenium derivatives. *ACS Mater. Lett.* **2022**, *4*, 440−447.
(38) Pratik, S. M.; Coropceanu, V.; Brédas, J. L. Enhancement of Thermally Activated Delayed Fluorescence (TADF) in Multi-Resonant Emitters via Control of Chalcogen Atom Embedding. *Chem. Mater.* **2022**, *34*, 8022−8030.
(39) Bhattacharyya, K. Can TDDFT render the electronic excited states ordering of Azine derivative? A closer investigation with DLPNO-STEOM-CCSD. *Chem. Phys. Lett.* **2021**, *779*, 138827.
(40) Wang, X.; Gao, S.; Zhao, M.; Marom, N. Benchmarking time-dependent density functional theory for singlet excited states of thermally activated delayed fluorescence chromophores. *Phys. Rev. Res.* **2022**, *4*, 033147.
(41) Goerigk, L.; Grimme, S. Double-hybrid density functionals. *Wiley Interdiscip. Rev. Comput. Mol. Sci.* **2014**, *4*, 576−600.
(42) Pollice, R.; Friederich, P.; Lavigne, C.; Gomes, G. d. P.; Aspuru-Guzik, A. Organic molecules with inverted gaps between first excited singlet and triplet states and appreciable fluorescence rates. *Matter* **2021**, *4*, 1654−1682.
(43) Casanova-Páez, M.; Dardis, M. B.; Goerigk, L. ωB2PLYP and ωB2GPPLYP: the first two double-hybrid density functionals with long-range correction optimized for excitation energies. *J. Chem. Theory Comput.* **2019**, *15*, 4735−4744.
(44) Frisch, M. J.; Trucks, G. W.; Schlegel, H. B.; Scuseria, G. E.; Robb, M. A.; Cheeseman, J. R.; Scalmani, G.; Barone, V.; Mennucci, B.; Petersson, G. A. et al. *Gaussian 09* Revision E.01.; Gaussian Inc.: Wallingford CT, 2009.
(45) (a) Barone, V. Geometry optimization of molecular structures in solution by the polarizable continuum model. *J. Comput. Chem.* **1998**, *19*, 404. (b) Barone, V.; Cossi, M. Quantum Calculation of Molecular Energies and Energy Gradients in Solution by a Conductor Solvent Model. *J. Phys. Chem. A* **1998**, *102*, 1995−2001.
(46) Gao, Y.; Pan, Q.-Q.; Zhao, L.; Geng, Y.; Su, T.; Gao, T.; Su, Z.-M. Realizing performance improvement of blue thermally activated delayed fluorescence molecule DABNA by introducing substituents on the para-position of boron atom. *Chem. Phys. Lett.* **2018**, *701*, 98−102.
(47) Konidena, R. K.; Naveen, K. R. Boron-Based Narrowband Multiresonance Delayed Fluorescent Emitters for Organic Light-Emitting Diodes. *Adv. Photonics Res.* **2022**, *3*, 2200201.
(48) Wu, X.; Su, B.-K.; Chen, D.-G.; Liu, D.; Wu, C.-C.; Huang, Z.-X.; Lin, T.-C.; Wu, C.-H.; Zhu, M.; Li, E. Y.; et al. The role of host−guest interactions in organic emitters employing MR-TADF. *Nat. Photonics* **2021**, *15*, 780−786.
(49) Ikeda, N.; Oda, S.; Matsumoto, R.; Yoshioka, M.; Fukushima, D.; Yoshiura, K.; Yasuda, N.; Hatakeyama, T. Solution-processable pure green thermally activated delayed fluorescence emitter based on the multiple resonance effect. *Adv. Mater.* **2020**, *32*, 2004072.
(50) Yuan, Y.; Tang, X.; Du, X.-Y.; Hu, Y.; Yu, Y.-J.; Jiang, Z.-Q.; Liao, L.-S.; Lee, S.-T. The design of fused amine/carbonyl system for efficient thermally activated delayed fluorescence: novel multiple resonance core and electron acceptor. *Adv. Opt. Mater.* **2019**, *7*, 1801536.
(51) Luo, X.-F.; Ni, H.-X.; Lv, A.-Q.; Yao, X.-K.; Ma, H.-L.; Zheng, Y.-X. High-Efficiency and Narrowband OLEDs from Blue to Yellow with Ternary Boron/Nitrogen-Based Polycyclic Heteroaromatic Emitters. *Adv. Opt. Mater.* **2022**, *10*, 2200504.
(52) Luo, X.; Zhang, L.; Zheng, Y.; Ding, L.; et al. Improving reverse intersystem crossing of MR-TADF emitters for OLEDs. *J. Semicond.* **2022**, *43*, 110202−110211.
(53) Wu, X.; Huang, J.-W.; Su, B.-K.; Wang, S.; Yuan, L.; Zheng, W.-Q.; Zhang, H.; Zheng, Y.-X.; Zhu, W.; Chou, P.-T. Fabrication of Circularly Polarized MR-TADF Emitters with Asymmetrical Peripheral-Lock Enhancing Helical B/N-Doped Nanographenes. *Adv. Mater.* **2022**, *34*, 2105080.
(54) Nagata, M.; Min, H.; Watanabe, E.; Fukumoto, H.; Mizuhata, Y.; Tokitoh, N.; Agou, T.; Yasuda, T. Fused-Nonacyclic Multi-Resonance Delayed Fluorescence Emitter Based on Ladder-Thiaborin Exhibiting Narrowband Sky-Blue Emission with Accelerated Reverse Intersystem Crossing. *Angew. Chem.* **2021**, *133*, 20442−20447.
(55) Knöller, J. A.; Meng, G.; Wang, X.; Hall, D.; Pershin, A.; Beljonne, D.; Olivier, Y.; Laschat, S.; Zysman-Colman, E.; Wang, S. Intramolecular borylation via sequential B- Mes bond cleavage for the divergent synthesis of B, N, B-doped benzo [4] helicenes. *Angew. Chem., Int. Ed.* **2020**, *59*, 3156−3160.
(56) Hirai, H.; Nakajima, K.; Nakatsuka, S.; Shiren, K.; Ni, J.; Nomura, S.; Ikuta, T.; Hatakeyama, T. One-step borylation of 1, 3-diaryloxybenzenes towards efficient materials for organic light-emitting diodes. *Angew. Chem.* **2015**, *127*, 13785−13789.
(57) Xu, Y.; Cheng, Z.; Li, Z.; Liang, B.; Wang, J.; Wei, J.; Zhang, Z.; Wang, Y. Molecular-structure and device-configuration optimizations toward highly efficient green electroluminescence with narrowband emission and high color purity. *Adv. Opt. Mater.* **2020**, *8*, 1902142.

https://doi.org/10.1021/acs.jctc.3c01147
J. Chem. Theory Comput. XXXX, XXX, XXX−XXX

(58) Xiong, X.; Cheng, Y.-C.; Wang, K.; Yu, J.; Zhang, X.-H. A comparative study of two multi-resonance TADF analogous materials integrating chalcogen atoms of different periods. *Mater. Chem. Front.* **2023**, *7*, 929−936.
(59) Neese, F. The ORCA program system. *Wiley Interdiscip. Rev.: Comput. Mol. Sci.* **2012**, *2*, 73−78.
(60) Zhang, K.; Liu, J.; Zhang, Y.; Fan, J.; Wang, C.-K.; Lin, L. Theoretical study of the mechanism of aggregation-caused quenching in near-infrared thermally activated delayed fluorescence molecules: hydrogen-bond effect. *J. Phys. Chem. C* **2019**, *123*, 24705−24713.
(61) Xu, S.; Yang, Q.; Wan, Y.; Chen, R.; Wang, S.; Si, Y.; Yang, B.; Liu, D.; Zheng, C.; Huang, W. Predicting intersystem crossing efficiencies of organic molecules for efficient thermally activated delayed fluorescence. *J. Mater. Chem. C* **2019**, *7*, 9523−9530.
(62) Aizawa, N.; Harabuchi, Y.; Maeda, S.; Pu, Y.-J. Kinetic prediction of reverse intersystem crossing in organic donor−acceptor molecules. *Nat. Commun.* **2020**, *11*, 3909.
(63) Serdiuk, I. E.; Mońka, M.; Kozakiewicz, K.; Liberek, B.; Bojarski, P.; Park, S. Y. Vibrationally Assisted Direct Intersystem Crossing between the Same Charge-Transfer States for Thermally Activated Delayed Fluorescence: Analysis by Marcus−Hush Theory Including Reorganization Energy. *J. Phys. Chem. B* **2021**, *125*, 2696−2706.
(64) Dias, F. B.; Penfold, T. J.; Monkman, A. P. Photophysics of thermally activated delayed fluorescence molecules. *Methods Appl. Fluoresc.* **2017**, *5*, 012001.
(65) Kim, I.; Cho, K. H.; Jeon, S. O.; Son, W.-J.; Kim, D.; Rhee, Y. M.; Jang, I.; Choi, H.; Kim, D. S. Three states involving vibronic resonance is a key to enhancing reverse intersystem crossing dynamics of an organoboron-based ultrapure blue emitter. *J. Australas. Ceram. Soc.* **2021**, *1*, 987−997.
(66) Drummond, B. H.; Aizawa, N.; Zhang, Y.; Myers, W. K.; Xiong, Y.; Cooper, M. W.; Barlow, S.; Gu, Q.; Weiss, L. R.; Gillett, A. J.; et al. Electron spin resonance resolves intermediate triplet states in delayed fluorescence. *Nat. Commun.* **2021**, *12*, 4532.
(67) Stavrou, K.; Danos, A.; Hama, T.; Hatakeyama, T.; Monkman, A. Hot vibrational states in a high-performance multiple resonance emitter and the effect of excimer quenching on organic light-emitting diodes. *ACS Appl. Mater. Interfaces* **2021**, *13*, 8643−8655.
(68) Northey, T.; Penfold, T. The intersystem crossing mechanism of an ultrapure blue organoboron emitter. *Org. Electron.* **2018**, *59*, 45−48.
(69) Lu, T.; Chen, F. Multiwfn: A multifunctional wavefunction analyzer. *J. Comput. Chem.* **2012**, *33*, 580−592.
(70) Momma, K.; Izumi, F. *VESTA3* for three-dimensional visualization of crystal, volumetric and morphology data. *J. Appl. Crystallogr.* **2011**, *44*, 1272−1276.

https://doi.org/10.1021/acs.jctc.3c01147
J. Chem. Theory Comput. XXXX, XXX, XXX−XXX